Letter

Dineutron in the 2_1^+ state of ^{6}He

Shoya Ogawa* and Takuma Matsumoto†
Department of Physics, Kyushu University, Fukuoka 819-0395, Japan

(Received 8 November 2021; revised 9 March 2022; accepted 1 April 2022; published 14 April 2022)

We investigate the dineutron in the 2_1^+ state of ^{6}He via analysis of its decay mode by using the complex scaling method. In this Letter, we propose the cross section for the resonant state to distinguish the resonant contributions from the nonresonant ones. As a result, it is found that the shoulder peak appears in the cross section for the resonant state as a function of $\varepsilon_{n\text{-}n}$. Furthermore, we show that the $S = 0$ component of the cross section, where S is the total spin of the two valence neutrons, has a peak around the shoulder peak, which comes from the dineutron configuration in the 2_1^+ state. Thus we conclude that the shoulder peak is expected to indicate the existence of the dineutron in the 2_1^+ state.

DOI: 10.1103/PhysRevC.105.L041601

Introduction. Neutron-rich nuclei have been intensively pursued since the development of radioactive ion-beam experiments. Two-neutron halo nuclei appear near the neutron drip line and have two loosely bound neutrons surrounding a core nucleus. A property of two-neutron halo nuclei is that the structure is described by a $n + n +$ core three-body system, referred to as the Borromean structure, which has no bound subsystems. Besides, there is only one bound state, i.e., the ground state. In the ground state of two-neutron halo nuclei, existence of the dineutron, which is a spatially compact two-neutron pair, has been predicted in various theoretical calculations [1–14]. Recently, it has been clarified that the dineutron develops in the surface region of ^{11}Li by an experiment for the knockout reaction [12]. Furthermore, experimental studies for Coulomb breakup reactions indicate the existence of the dineutron in the ground states of ^{6}He [13] and ^{19}B [14].

Excited states of two-neutron halo nuclei appear above the three-body threshold as resonant states. The resonant states are unbound states and decay into three particles, namely, two neutrons and a core nucleus. Elucidation of some resonant states, e.g., the 2_1^+ state in ^{6}He [15] and unbound nuclei ^{6}Be [16–18], ^{16}Be [17,19], and ^{26}O [20,21], have attracted much attention and have been investigated via decay-particle measurements, which include information on the structure. However, the decay observables, such as excitation energy spectra of the cross section, contain not only the resonant contribution but also contributions from the nonresonant states. To investigate structural information of the resonant states, we need to eliminate the nonresonant contributions from the cross section [22]. This point makes it difficult to clarify properties of the resonant states.

^{6}He is the lightest two-neutron halo nucleus and has been investigated intensively so far [13,23–33]. In Ref. [15], the 2_1^+ resonant state of ^{6}He was investigated via the $^6\text{He} + ^{12}\text{C}$ reaction at 240 MeV/nucleon [23]. In previous work, the double-differential breakup cross section (DDBUX) with respect to the two-neutron relative energy ($\varepsilon_{n\text{-}n}$) and the energy between the centers of mass (c.m.) of the two-neutron system and α ($\varepsilon_{nn\text{-}\alpha}$) was calculated by combining the continuum discretized coupled channels (CDCC) method [34] with the complex-scaled Lippmann-Schwinger (CSLS) equation [10,11]. Furthermore, to extract the contribution from the resonant state, they calculated the breakup cross section as a function of $\varepsilon_{n\text{-}n}$, $d\sigma/d\varepsilon_{n\text{-}n}$, by gating the total excited energy of ^{6}He within the range of the energy of the 2_1^+ state, where the DDBUX was integrated over $\varepsilon_{nn\text{-}\alpha}$. According to the results, the shoulder peak appears in $d\sigma/d\varepsilon_{n\text{-}n}$ around 0.8 MeV. They suggested that the shoulder peak indicates the existence of the dineutron in the 2_1^+ state. Recently the structure has attracted much attention because the experimental study [35] reported the observation of the shoulder peak.

Although the cross section is gated within the resonant energy, it cannot completely exclude the nonresonant contributions from the cross section. Therefore, the evidence of the dineutron in the 2_1^+ state is insufficient at this stage. To clarify this point, it is necessary to isolate a resonant state in multichannel systems and analyze its contribution to the cross section. In order to calculate the resonant states, various approaches have been used so far, such as the complex scaling method (CSM) [36–38] and methods based on the hyperspherical coordinate [19,27,39,40]. In this study, we propose a method of extracting only the resonant contribution from the cross section by using the CSM. In the CSM, the resonant state can be completely separated from the nonresonant state. Therefore we can evaluate the cross section to the resonant state calculated by the CSM.

In this Letter, the dineutron in the 2_1^+ state of ^{6}He is investigated via the analysis of the $^6\text{He} + ^{12}\text{C}$ reaction at

*s-ogawa@phys.kyushu-u.ac.jp
†matsumoto@phys.kyushu-u.ac.jp

240 MeV/nucleon in a framework combining the CDCC with the CSLS. The reaction is described as a $n+n+\alpha+{}^{12}\mathrm{C}$ four-body system, and the 2_1^+ state is obtained by the CSM. In this analysis, we calculate the DDBUX and $d\sigma/d\varepsilon_{n\text{-}n}$ for the resonant contribution and discuss the dineutron configuration in the 2_1^+ state.

Formalism. The ${}^6\mathrm{He}+{}^{12}\mathrm{C}$ system is described as a four-body breakup reaction, and the Schrödinger equation is written as

$$[K_R + U + h - E]|\Psi^{(+)}\rangle = 0, \tag{1}$$

with

$$U = U_n + U_n + U_\alpha + V_\mathrm{C}, \tag{2}$$

where $\boldsymbol{R}$ represents the coordinate between the c.m. of ${}^6\mathrm{He}$ and ${}^{12}\mathrm{C}$. K_R is the kinetic energy operator associated with $\boldsymbol{R}$, and h is the internal Hamiltonian of ${}^6\mathrm{He}$. U_n (U_α) describes the optical potential between n (α) and ${}^{12}\mathrm{C}$. These potentials are obtained by the folding model with the Melbourne g matrix [41] in the same manner as used in Ref. [42]. V_C is the Coulomb potential between the c.m. of ${}^6\mathrm{He}$ and ${}^{12}\mathrm{C}$, that is, Coulomb breakup is neglected in this study.

The CDCC equation is constructed within the model space $\mathcal{P}$ as

$$\mathcal{P}[K_R + U + h - E]\mathcal{P}|\Psi^{(+)}\rangle = 0, \tag{3}$$

where $\mathcal{P}$ is defined by

$$\mathcal{P} = \sum_n |\Phi_n\rangle\langle\Phi_n| . \tag{4}$$

A set of eigenstates $\{\Phi_n\}$ is obtained by diagonalizing h with the Gaussian expansion method (GEM) [43] and includes the bound and discretized continuum states. In the CDCC, the transition matrix to the discretized state is represented as

$$T_n = \langle \Phi_n \chi_n^{(-)}(\boldsymbol{P}_n)|U - V_\mathrm{C}|\mathcal{P}\Psi^{(+)}\rangle , \tag{5}$$

where $\chi_n^{(-)}(\boldsymbol{P}_n)$ is the Coulomb wave function with the asymptotic relative momentum $\boldsymbol{P}_n$ and satisfies the incoming boundary condition. Using the smoothing procedure with the CSLS [15], the continuous transition matrix is calculated as

$$T_\varepsilon(\boldsymbol{k},\boldsymbol{K},\boldsymbol{P}) = \sum_n f_{\varepsilon,n}(\boldsymbol{k},\boldsymbol{K})T_n, \tag{6}$$

with the smoothing function defined as

$$f_{\varepsilon,n}(\boldsymbol{k},\boldsymbol{K}) = \langle \Phi_\varepsilon^{(-)}(\boldsymbol{k},\boldsymbol{K})|\Phi_n\rangle . \tag{7}$$

Here $\Phi_\varepsilon^{(-)}$ is the three-body scattering wave function of ${}^6\mathrm{He}$ with the internal energy ε and satisfies the incoming boundary condition. The asymptotic relative momentum regarding $\boldsymbol{R}$ is represented by $\boldsymbol{P}$, and the asymptotic internal momenta of $\boldsymbol{k}$ and $\boldsymbol{K}$ in ${}^6\mathrm{He}$ satisfy the relation $\varepsilon = (\hbar^2k^2)/(2\mu_{n\text{-}n}) + (\hbar^2K^2)/(2\mu_{nn\text{-}\alpha})$, where $\mu_{n\text{-}n}$ and $\mu_{nn\text{-}\alpha}$ are the reduced masses of the n-n and nn-α systems, respectively.

To calculate $f_{\varepsilon,n}(\boldsymbol{k},\boldsymbol{K})$, we apply the CSLS that describes the three-body scattering wave function with the appropriate boundary condition:

$$f_{\varepsilon,n}(\boldsymbol{k},\boldsymbol{K}) = \langle\phi(\boldsymbol{k},\boldsymbol{K})|\,\Phi_n\rangle + \sum_\nu \langle\phi(\boldsymbol{k},\boldsymbol{K})|V U_\theta^{-1}\big|\Phi_\nu^\theta\big\rangle \frac{1}{\varepsilon-\varepsilon_\nu^\theta}\big\langle\tilde\Phi_\nu^\theta\big|\,U_\theta|\Phi_n\rangle, \tag{8}$$

where ϕ represents the plane wave for three-body scattering. V is the sum of the interactions in h. U_θ is the scaling transformation operator in the CSM. The νth eigenstate with the eigenenergy ε_ν^θ calculated by the CSM is represented by Φ_ν^θ. It should be noted that a set of eigenstates $\{\Phi_\nu^\theta\}$ forms a complete set as $\sum_\nu |\Phi_\nu^\theta\rangle\langle\tilde\Phi_\nu^\theta| = 1$, which is referred to as an extended completeness relation [44–46]. Furthermore, combining $U_\theta^{-1}U_\theta = 1$ with the extended completeness relation, we obtain $\sum_\nu U_\theta^{-1}|\Phi_\nu^\theta\rangle\langle\tilde\Phi_\nu^\theta|\,U_\theta = 1$.

Using Eq. (6), the DDBUX with respect to $\varepsilon_{n\text{-}n}$ and $\varepsilon_{nn\text{-}\alpha}$ is calculated as

$$\frac{d^2\sigma}{d\varepsilon_{n\text{-}n}d\varepsilon_{nn\text{-}\alpha}} = \sum_n\sum_{n'} T_n^\dagger T_{n'} \times \int d\boldsymbol{k}d\boldsymbol{K}d\boldsymbol{P}\, f_{\varepsilon,n}^\dagger(\boldsymbol{k},\boldsymbol{K}) f_{\varepsilon,n'}(\boldsymbol{k},\boldsymbol{K}) \times \delta\left(E_\mathrm{tot} - \frac{\hbar^2\boldsymbol{P}^2}{2\mu_R} - \varepsilon_{n\text{-}n} - \varepsilon_{nn\text{-}\alpha}\right) \times \delta\left(\varepsilon_{n\text{-}n} - \frac{\hbar^2\boldsymbol{k}^2}{2\mu_{n\text{-}n}}\right)\delta\left(\varepsilon_{nn\text{-}\alpha} - \frac{\hbar^2\boldsymbol{K}^2}{2\mu_{nn\text{-}\alpha}}\right), \tag{9}$$

where E_tot is the total energy of the reaction system, and μ_R is the reduced mass of the ${}^6\mathrm{He}+{}^{12}\mathrm{C}$ system.

To extract the resonant contribution from Eq. (9), we consider the transition matrix to Φ_ν^θ, which is separated into the resonant and nonresonant states. Inserting $\sum_\nu U_\theta^{-1}|\Phi_\nu^\theta\rangle\langle\tilde\Phi_\nu^\theta|\,U_\theta = 1$ into Eq. (6), the continuous transition matrix and its Hermitian conjugate are rewritten as

$$T_\varepsilon(\boldsymbol{k},\boldsymbol{K},\boldsymbol{P}) = \sum_\nu f_{\varepsilon,\nu}^\theta(\boldsymbol{k},\boldsymbol{K})\tilde T_\nu^\theta, \tag{10}$$

with

$$\tilde T_\nu^\theta = \sum_n \big\langle\tilde\Phi_\nu^\theta\big|U_\theta|\Phi_n\rangle\, T_n, \quad f_{\varepsilon,\nu}^\theta = \langle\Phi_\varepsilon^{(-)}|U_\theta^{-1}\big|\Phi_\nu^\theta\big\rangle. \tag{11}$$

In Eq. (11), the arguments of $\boldsymbol{k}$ and $\boldsymbol{K}$ are omitted for simplicity. T_ν^θ, which has the same definition in Ref. [47], can be interpreted as the transition matrix to Φ_ν^θ. Using Eq. (10), Eq. (9) is rewritten as the following summation for ν:

$$\frac{d^2\sigma}{d\varepsilon_{n\text{-}n}d\varepsilon_{nn\text{-}\alpha}} = \sum_\nu\sum_{\nu'} T_\nu^{\theta\dagger}T_{\nu'}^\theta \times \int d\boldsymbol{k}\,d\boldsymbol{K}\,d\boldsymbol{P}\, f_{\varepsilon,\nu}^{\theta\dagger}(\boldsymbol{k},\boldsymbol{K}) f_{\varepsilon,\nu'}^\theta(\boldsymbol{k},\boldsymbol{K})\delta_\mathrm{e.c.}, \tag{12}$$

where $\delta_\mathrm{e.c.}$ represents a set of the three δ functions in Eq. (9). We confirm that the result of Eq. (12) is consistent with that of

Eq. (9). In this study, we define the DDBUX for the resonant state as

$$\frac{d^2\sigma_{\nu_R}}{d\varepsilon_{n\text{-}n}d\varepsilon_{nn\text{-}\alpha}} \equiv T^{\theta\dagger}_{\nu_R} T^{\theta}_{\nu_R} \times \int d\boldsymbol{k}\, d\boldsymbol{K}\, d\boldsymbol{P}\, f^{\theta\dagger}_{\varepsilon,\nu_R}(\boldsymbol{k},\boldsymbol{K}) f^{\theta}_{\varepsilon,\nu_R}(\boldsymbol{k},\boldsymbol{K})\delta_{\text{e.c.}}, \tag{13}$$

where ν_R represents the resonant state 2_1^+ with the resonant energy ε_r and decay width Γ. This cross section is referred as the *resonant cross section* in this Letter.

In this study, we apply the same internal Hamiltonian h as used in Ref. [22]. As a model space for the total spin I and the parity π in ^{6}He, we take $I^\pi = 0^+, 1^-$, and 2^+. The particle exchange between valence neutrons and neutrons in α is treated with the orthogonality condition model [48]. In the GEM, we take the Gaussian range parameters r_i $(i = 1, 2, \ldots, N)$ that lie in geometric progression. We adopt the same parameters in Ref. [15] for Φ_n. For $\Phi_{\theta,\nu}$ in the CSLS and $\Phi^{\theta}_{\nu_R}$, $(N, r_1, r_N) = (22, 0.1\text{ fm}, 75\text{ fm})$ and $(16, 0.1\text{ fm}, 25\text{ fm})$ are taken, respectively. As a result, we obtain the ground state energy -0.972 MeV and $(\varepsilon_r, \Gamma) = (0.823\text{ MeV}, 0.121\text{ MeV})$ for the 2_1^+. The scaling angle θ is set to 12°. The convergence of the calculated cross section has been achieved within about 5% fluctuation.

Results and discussions. First, to discuss the dineutron in the 2_1^+ state, we consider the angular density as

$$\rho(\theta_{12}) \equiv \left\langle \tilde{\Phi}^{\theta}_{\nu_R} \middle| \delta(\omega - \theta_{12}) \middle| \Phi^{\theta}_{\nu_R} \right\rangle, \tag{14}$$

where θ_{12} is the opening angle between the two valence neutrons. This density is normalized as $\int \rho(\theta_{12}) d\theta_{12} = 1$ and is independent of the scaling angle in the CSM. The details of $\rho(\theta_{12})$ are discussed in Ref. [49]. Here it should be noted that the angular density of a resonant state is complex because an expected value for a resonant state is defined in the framework of non-Hermitian quantum mechanics [50]. According to Ref. [51], the real part means the expected value of an operator, and the imaginary part, which comes from the interference between the resonant state and nonresonant states, corresponds to the uncertainty of the expected value.

In Fig. 1(a), we demonstrate the angular density of the ground state represented by the solid line, which shows the two peaks at the small and large angles. The peak at the small angle indicates the dineutron configuration because the small angle means a short distance between the two valence neutrons. To discuss this behavior in more detail, we separate the angular density into the $S = 0$ and 1 components, where S represents the total spin of the two valence neutrons. The dotted and dot-dashed lines represent the angular density for $S = 0$ and 1, respectively. One sees that the $S = 0$ component has also the two peaks at the small and large angles, and the $S = 1$ component behaves almost symmetrically. Therefore, the dineutron is formed in the case for $S = 0$.

The solid line in Fig. 1(b) represents the real part of the angular density of the 2_1^+ state, and it takes the maximum

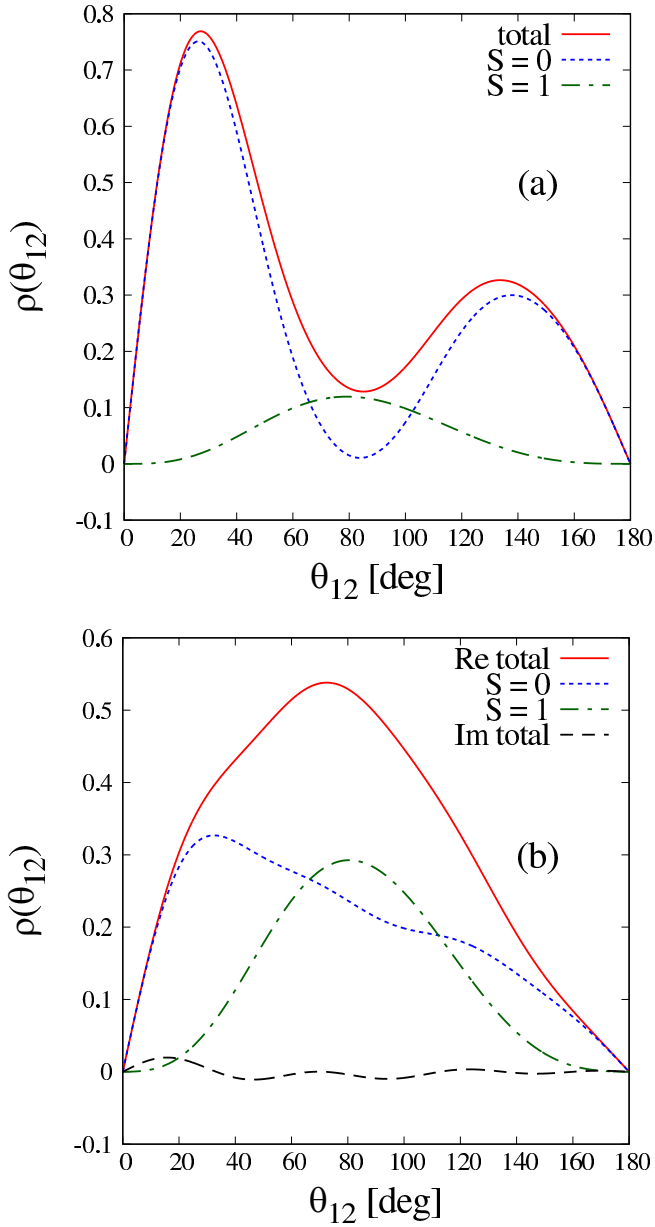

FIG. 1. The angular density of (a) the ground state and (b) the 2_1^+ state. This density is a function of the opening angle between the two valence neutrons.

value in the region $\theta_{12} = 60$–80°. Since the imaginary part of $\rho(\theta_{12})$ shown by the dashed line is negligibly small, we discuss only the real part of $\rho(\theta_{12})$. The dotted and dot-dashed lines represent the angular density for $S = 0$ and 1, respectively. One can see that the $S = 0$ component has a peak structure at the small angle. Therefore the dineutron in the 2_1^+ state is expected to be clear when we focus on the $S = 0$ component. Next we discuss the DDBUX for the $^6\text{He} + ^{12}\text{C}$ reaction at 240 MeV/nucleon. Figure 2(a) shows the DDBUX describing the transition to the 2^+ continuum states calculated with Eq. (9). In this analysis, the OCM is not included in V for Eq. (8) because we avoid the instability of numerical results as mentioned in Ref. [52]. The peak structure can be seen when

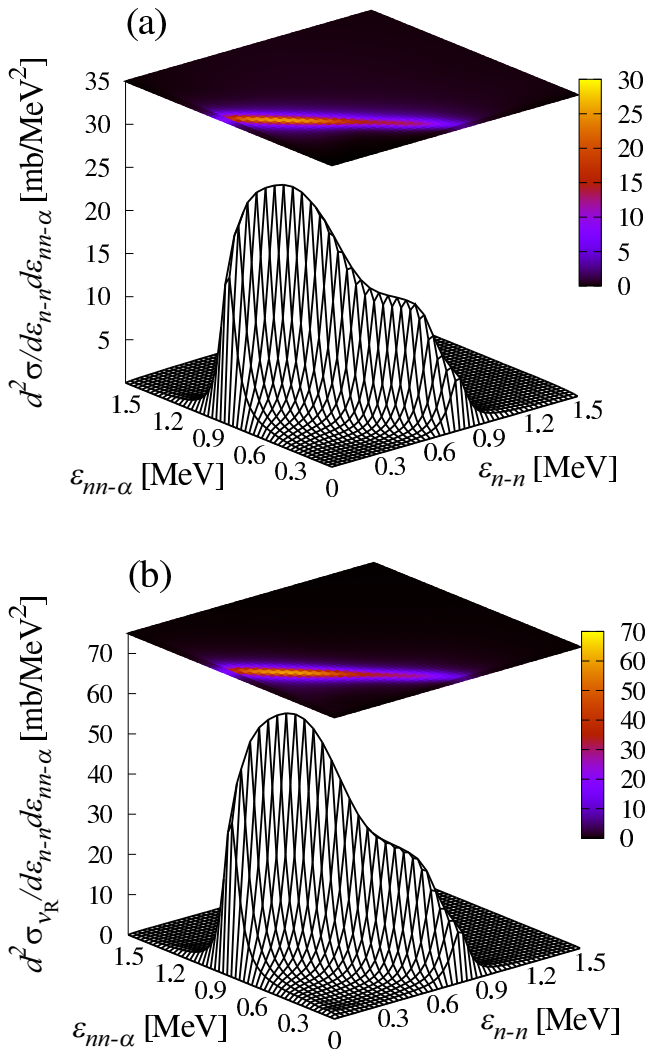

FIG. 2. The breakup cross sections describing the transition to (a) the 2^+ continuum states calculated with Eq. (9) and (b) the 2^+_1 state calculated with Eq. (13). Here the panel (b) shows the real part of DDBUX.

ε $(= \varepsilon_{n\text{-}n} + \varepsilon_{nn\text{-}\alpha})$ is around 0.8 MeV, which corresponds to the resonant energy of the 2^+_1 state. This behavior is the same as shown in Fig. 1(b) of Ref. [15]. Moreover, as shown in Fig. 2(b), one clearly sees that the behavior of the DDBUX for the 2^+_1 calculated by using the resonant cross section is similar to one in Fig. 2(a). It should be noted that the absolute value of Fig. 2(b) is larger than the one of Fig. 2(a). The large absolute value can be reduced by the contributions from the interference between the resonant state and nonresonant states as discussed later. In order to investigate the dineutron in the 2^+_1 state, we calculate the cross section with respect to the $\varepsilon_{n\text{-}n}$ as

$$\frac{d\sigma_{\nu_R}}{d\varepsilon_{n\text{-}n}} \equiv \int_D \frac{d^2\sigma_{\nu_R}}{d\varepsilon_{n\text{-}n}d\varepsilon_{nn\text{-}\alpha}} d\varepsilon_{nn\text{-}\alpha} \quad (D : \varepsilon_r - \Gamma/2 \leqslant \varepsilon_{n\text{-}n} + \varepsilon_{nn\text{-}\alpha} \leqslant \varepsilon_r + \Gamma/2). \quad (15)$$

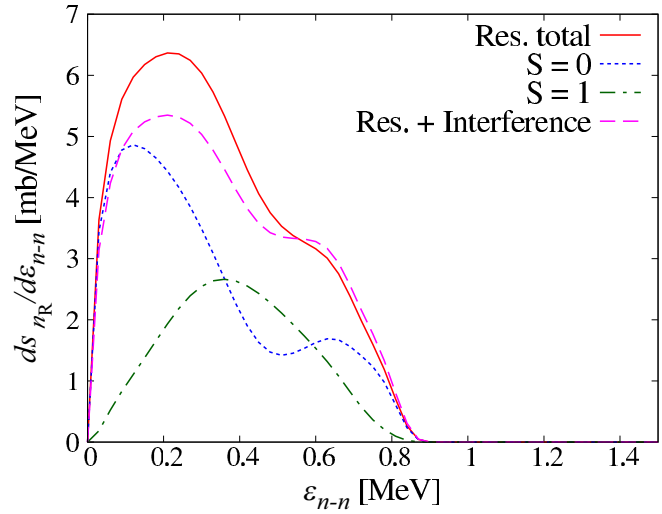

FIG. 3. The breakup cross section with respect to $\varepsilon_{n\text{-}n}$ calculated by using Eq. (15).

This cross section shows the energy distribution of the two valence neutrons decaying from the resonant state. In Fig. 3, the solid line shows the cross section, and the same two peaks discussed in the previous study [15] are seen. One is the clear peak around 0.2 MeV and the other is the shoulder peak around 0.7 MeV, which is mentioned as the contribution from the dineutron in the 2^+_1 state. Because the cross section in Fig. 3 is reduced from only the 2^+_1 state, we can conclude that the shoulder peak confirmed in the previous study comes from the 2^+_1 state, not the nonresonant states.

To investigate the shoulder peak in more detail, we separate the cross section into the $S = 0$ and 1 components. To this end, the scattering wave function is represented as follows

$$\langle \Phi^{(-)}_{\varepsilon}(\boldsymbol{k}, \boldsymbol{K})| = \langle \Phi^{(-)}_{\varepsilon,S=0}(\boldsymbol{k}, \boldsymbol{K})| + \langle \Phi^{(-)}_{\varepsilon,S=1}(\boldsymbol{k}, \boldsymbol{K})|\,, \quad (16)$$

where $\Phi^{(-)}_{\varepsilon,S}$ $(S = 0, 1)$ describes that the two neutrons have the total spin S in the asymptotic region. Using Eq. (16), Eq. (15) is rewritten as

$$\frac{d\sigma_{\nu_R}}{d\varepsilon_{n\text{-}n}} = \left(\frac{d\sigma_{\nu_R}}{d\varepsilon_{n\text{-}n}}\right)_{S=0} + \left(\frac{d\sigma_{\nu_R}}{d\varepsilon_{n\text{-}n}}\right)_{S=1}, \quad (17)$$

where $(d\sigma_{\nu_R}/d\varepsilon_{n\text{-}n})_S$ corresponds to the cross section obtained by replacing the $\Phi^{(-)}_{\varepsilon}$ in Eq. (11) with $\Phi^{(-)}_{\varepsilon,S}$. The dotted and dot-dashed lines show the $S = 0$ and 1 components, respectively. One can see that the $S = 0$ component has two peaks. The first peak around 0.2 MeV contributes to the clear peak of the total component, and the second peak around 0.7 MeV has effects on the shoulder peak. For the second peak, the two-neutron pair has a relatively large momentum that means a spatially compact pair in the coordinate space. Consequently we can conclude that the shoulder peak indicates the existence of the dineutron in the 2^+_1 state.

Furthermore, to discuss the large absolute value of the resonant cross section, we calculate the breakup cross section for

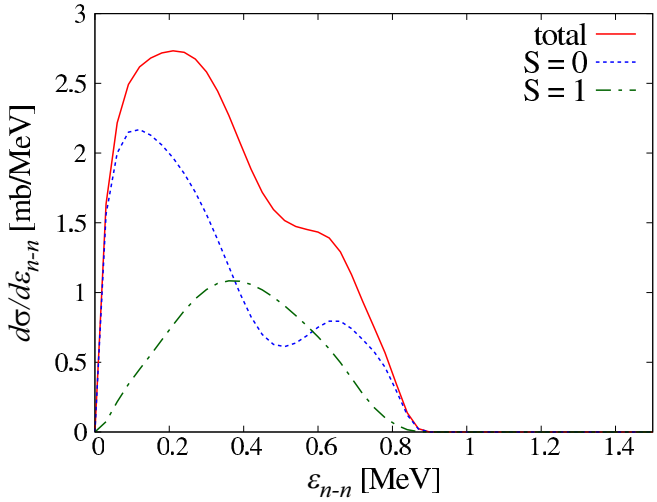

FIG. 4. The breakup cross section with respect to $\varepsilon_{n\text{-}n}$ calculated by using Eq. (19).

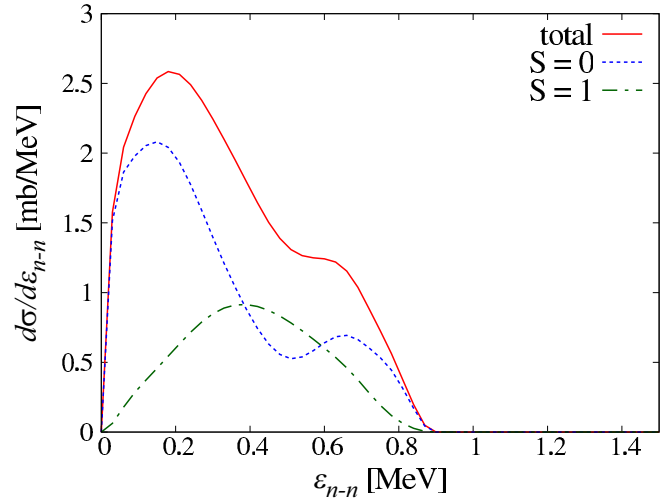

FIG. 5. Same as Fig. 4, but with the Gogny-Pires-Tourreil interaction as v_{nn}.

the interference between the resonant and nonresonant states defined as

$$\left(\frac{d\sigma}{d\varepsilon_{n\text{-}n}}\right)_{\text{interference}} \equiv \int_D d\varepsilon_{nn\text{-}\alpha}\, 2\,\mathrm{Re}\left[\sum_{\nu\in D'} T_\nu^{\theta\dagger} T_{\nu_\mathrm{R}}^{\theta} \times \int d\boldsymbol{k} d\boldsymbol{K}\, d\boldsymbol{P}\, f_{\varepsilon,\nu}^{\theta\dagger}(\boldsymbol{k},\boldsymbol{K}) f_{\varepsilon,\nu_\mathrm{R}}^{\theta}(\boldsymbol{k},\boldsymbol{K})\delta_{\text{e.c.}}\right]$$

$$(D' : \varepsilon_r - \Gamma/2 \leqslant \mathrm{Re}[\varepsilon_\nu^\theta] \leqslant \varepsilon_r + \Gamma/2,\ \ \nu \neq \nu_R). \quad (18)$$

Here ν satisfies the region D', that is, Eq. (18) gives the interference from the nonresonant states near the resonant energy of the 2_1^+ state. The dashed line in Fig. 3 means the sum of the solid line and Eq. (18). Therefore the effect of the interference reduces the breakup cross section without changing its shape. In this analysis, we confirmed that the nonresonant contributions, which are the terms for $\nu = \nu' \neq \nu_\mathrm{R}$ in Eq. (12), and the interference between the nonresonant states are negligible. Further the absolute value of the dashed line would be smaller when we expand the region D'. Next, to evaluate the contribution from the dineutron in the 2_1^+ state on the cross section, which can be observed practically, we calculate the cross section with respect to $\varepsilon_{n\text{-}n}$ defined in Ref. [15] as

$$\frac{d\sigma_{2_1^+}}{d\varepsilon_{n\text{-}n}} \equiv \int_D \frac{d^2\sigma}{d\varepsilon_{n\text{-}n} d\varepsilon_{nn\text{-}\alpha}} d\varepsilon_{nn\text{-}\alpha}. \quad (19)$$

Here $d^2\sigma/d\varepsilon_{n\text{-}n}d\varepsilon_{nn\text{-}\alpha}$ is the component of the 2^+ continuum states as shown in Fig. 2(a). In Fig. 4, the solid line describes the obtained cross section, and the shoulder peak is also seen in the present result. The dotted and dot-dashed lines represent the results of the $S = 0$ and 1 components, respectively. The behavior of the cross section in Fig. 4 is consistent with that in Fig. 3. Thus the cross section gated within the resonant energy region corresponds to that for the resonant state.

Finally, we investigate the dependence of the dineutron structure on the interaction between the two neutrons v_{nn} in ^{6}He. As another v_{nn}, we use the Gogny-Pires-Tourreil interaction [53], which has been successful in several three-body calculations for core + n + n [2,54,55]. In Fig. 5, the solid line shows the breakup cross section calculated with Eq. (19). The dotted and dot-dashed lines represent the $S = 0$ and 1 components, respectively. One can see the same shoulder peak as the one obtained with the Minnesota interaction as v_{nn}. Thus the dineutron structure appears in the 2_1^+ state with the reliable v_{nn}. Furthermore we confirm that the optical potential does not depend on the dineutron structure because the T matrix including the effect of the optical potential is just a constant coefficient of the resonant cross section.

Summary. We analyzed the DDBUX of the $^6\mathrm{He} + ^{12}\mathrm{C}$ reaction at 240 MeV/nucleon to investigate the dineutron in the resonant state 2_1^+. To eliminate the nonresonant contribution from the DDBUX, we defined the DDBUX for the resonant state by reconstructing the transition matrix with the extended completeness relation in the CSM. The calculated cross section for the resonant state as a function of $\varepsilon_{n\text{-}n}$ has the shoulder peak, which is discussed as the contribution from the dineutron. Thus we found that the shoulder peak comes from the resonant state, not nonresonant state. Furthermore, we separated the cross section into the $S = 0$ and 1 components. As a result, the $S = 0$ component of the cross section has the second peak around the shoulder peak. In the second peak, the two-neutron pair has a relatively large momentum that corresponds to a spatially compact configuration between the two neutrons. Therefore the shoulder peak is expected to indicate the existence of the dineutron in the 2_1^+ state, and the dineutron structure does not depend on v_{nn} and the optical potential. In the cross section, which can be observed practically, the same peak is confirmed in the $S = 0$ component. These results strongly support the suggestion in the previous study. Recently, new experimental data for $^6\mathrm{He} + ^{12}\mathrm{C}$ reaction system [35] showed the shoulder peak, and our calculations thus play an important role in understanding the data.

One of the important points of this study is that we can investigate the structure of a resonant state by using the resonant cross section. In addition, the shape of the resonant cross section does not depend on the reaction system because the T matrix is just a constant coefficient for the resonant cross section. In a forthcoming paper, we analyze several resonant states of other two-neutron halo nuclei, such as ^{11}Li, ^{14}Be, and ^{22}C, by using the resonant cross section.

Acknowledgments. The authors would like to thank Prof. Kikuchi for fruitful discussions. This work is supported in part by Grant-in-Aid for Scientific Research (No. JP18K03650) from the Japan Society for the Promotion of Science (JSPS).

[1] Y. T. Oganessian, V. I. Zagrebaev, and J. S. Vaagen, Phys. Rev. Lett. **82**, 4996 (1999).
[2] M. V. Zhukov *et al.*, Phys. Rep. **231**, 151 (1993).
[3] G. F. Bertsch and H. Esbensen, Ann. Phys. (NY) **209**, 327 (1991).
[4] H. Esbensen and G. F. Bertsch, Phys. Rev. C **59**, 3240 (1999).
[5] K. Hagino and H. Sagawa, Phys. Rev. C **72**, 044321 (2005).
[6] K. Hagino, H. Sagawa, T. Nakamura, and S. Shimoura, Phys. Rev. C **80**, 031301(R) (2009).
[7] J. Singh *et al.*, Phys. Rev. C **101**, 024310 (2020).
[8] J. Casal, J. Singh, L. Fortunato, W. Horiuchi, and A. Vitturi, Phys. Rev. C **102**, 064627 (2020).
[9] G. Papadimitriou, A. T. Kruppa, N. Michel, W. Nazarewicz, M. Płoszajczak, and J. Rotureau, Phys. Rev. C **84**, 051304(R) (2011).
[10] Y. Kikuchi, K. Katō, T. Myō, M. Takashina, and K. Ikeda, Phys. Rev. C **81**, 044308 (2010).
[11] Y. Kikuchi *et al.*, Prog. Theor. Exp. Phys. **2016**, 103D03 (2016).
[12] Y. Kubota *et al.*, Phys. Rev. Lett. **125**, 252501 (2020).
[13] Y. L. Sun *et al.*, Phys. Lett. B **814**, 136072 (2021).
[14] K. J. Cook *et al.*, Phys. Rev. Lett. **124**, 212503 (2020).
[15] Y. Kikuchi, T. Matsumoto, K. Minomo, and K. Ogata, Phys. Rev. C **88**, 021602(R) (2013).
[16] T. Oishi, K. Hagino, and H. Sagawa, Phys. Rev. C **90**, 034303 (2014).
[17] J. Casal, Phys. Rev. C **97**, 034613 (2018).
[18] S. M. Wang and W. Nazarewicz, Phys. Rev. Lett. **126**, 142501 (2021).
[19] A. E. Lovell, F. M. Nunes, and I. J. Thompson, Phys. Rev. C **95**, 034605 (2017).
[20] K. Hagino and H. Sagawa, Phys. Rev. C **89**, 014331 (2014).
[21] K. Hagino and H. Sagawa, Phys. Rev. C **93**, 034330 (2016).
[22] S. Ogawa and T. Matsumoto, Phys. Rev. C **102**, 021602(R) (2020).
[23] T. Aumann, D. Aleksandrov, L. Axelsson, T. Baumann, M. J. G. Borge, L. V. Chulkov, J. Cub, W. Dostal, B. Eberlein, T. W. Elze, H. Emling, H. Geissel, V. Z. Goldberg, M. Golovkov, A. Grunschloss, M. Hellstrom, K. Hencken, J. Holeczek, R. Holzmann, B. Jonson *et al.*, Phys. Rev. C **59**, 1252 (1999).
[24] S. Bacca, M. A. Marchisio, N. Barnea, W. Leidemann, and G. Orlandini, Phys. Rev. Lett. **89**, 052502 (2002).
[25] T. Matsumoto, E. Hiyama, K. Ogata, Y. Iseri, M. Kamimura, S. Chiba, and M. Yahiro, Phys. Rev. C **70**, 061601(R) (2004).
[26] M. Rodríguez-Gallardo, J. M. Arias, J. Gómez-Camacho, A. M. Moro, I. J. Thompson, and J. A. Tostevin, Phys. Rev. C **72**, 024007 (2005).
[27] P. Descouvemont, E. Tursunov, and D. Baye, Nucl. Phys. A **765**, 370 (2006).
[28] A. M. Moro, K. Rusek, J. M. Arias, J. Gómez-Camacho, and M. Rodríguez-Gallardo, Phys. Rev. C **75**, 064607 (2007).
[29] D. Baye, P. Capel, P. Descouvemont, and Y. Suzuki, Phys. Rev. C **79**, 024607 (2009).
[30] M. Brodeur, T. Brunner, C. Champagne, S. Ettenauer, M. J. Smith, A. Lapierre, R. Ringle, V. L. Ryjkov, S. Bacca, P. Delheij, G. W. F. Drake, D. Lunney, A. Schwenk, and J. Dilling, Phys. Rev. Lett. **108**, 052504 (2012).
[31] L. Acosta, A. M. Sanchez-Benitez, M. E. Gomez, I. Martel, F. Perez-Bernal, F. Pizarro, J. Rodriguez-Quintero, K. Rusek, M. A. G. Alvarez, M. V. Andres, J. M. Espino, J. P. Fernandez-Garcia, J. Gomez-Camacho, A. M. Moro, C. Angulo, J. Cabrera, E. Casarejos, P. Demaret, M. J. G. Borge, D. Escrig *et al.*, Phys. Rev. C **84**, 044604 (2011).
[32] L. Fortunato, R. Chatterjee, J. Singh, and A. Vitturi, Phys. Rev. C **90**, 064301 (2014).
[33] P. Descouvemont, Phys. Rev. C **93**, 034616 (2016).
[34] M. Yahiro *et al.*, Prog. Theor. Exp. Phys. **2012**, 01A206 (2012).
[35] A. Saito *et al.* (unpublished).
[36] J. Aguilar and J. M. Combes, Commun. Math. Phys. **22**, 269 (1971).
[37] E. Balslev and J. M. Combes, Commun. Math. Phys. **22**, 280 (1971).
[38] T. Myo *et al.*, Prog. Part. Nucl. Phys. **79**, 1 (2014).
[39] E. C. Pinilla and P. Descouvemont, Phys. Rev. C **94**, 024620 (2016).
[40] J. Casal and J. Gómez-Camacho, Phys. Rev. C **99**, 014604 (2019).
[41] K. Amos *et al.*, in *Advances in Nuclear Physics*, edited by J. W. Negele and E. Vogt (Plenum, New York, 2000), Vol. 25, p. 275.
[42] S. Ogawa *et al.*, Prog. Theor. Exp. Phys. **2019**, 123D04 (2019).
[43] E. Hiyama, Y. Kino, and M. Kamimura, Prog. Part. Nucl. Phys. **51**, 223 (2003).
[44] T. Myo, K. Katō, and A. Ohnishi, Prog. Theor. Phys. **99**, 801 (1998).
[45] B. Giraud and K. Katō, Ann. Phys. (NY) **308**, 115 (2003).
[46] B. Giraud, K. Katō, and A. Ohnishi, J. Phys. A: Math. Gen. **37**, 11575 (2004).
[47] T. Matsumoto, K. Katō, and M. Yahiro, Phys. Rev. C **82**, 051602(R) (2010).
[48] S. Saito, Prog. Theor. Phys. **41**, 705 (1969).
[49] A. T. Kruppa, G. Papadimitriou, W. Nazarewicz, and N. Michel, Phys. Rev. C **89**, 014330 (2014).
[50] N. Moiseyev, *Non-Hermitian Quantum Mechanics* (Cambridge University Press, Cambridge, 2011).
[51] T. Berggren, Phys. Lett. B **373**, 1 (1996).
[52] Y. Kikuchi *et al.*, Prog. Theor. Phys. **122**, 499 (2009).
[53] D. Gogny, P. Pires, and R. De Tourreil, Phys. Lett. B **32**, 591 (1970).
[54] I. Thompson, F. Nunes, and B. Danilin, Comput. Phys. Commun. **161**, 87 (2004).
[55] J. Casal, M. Rodriguez-Gallardo, and J. M. Arias, Phys. Rev. C **88**, 014327 (2013).